



# Optimising power take-off of an oscillating wave surge converter using high fidelity numerical simulations



Pál Schmitt<sup>a,\*</sup>, Henrik Asmuth<sup>b</sup>, Björn Elsässer<sup>a</sup>

<sup>a</sup> Marine Research Group, Queen's University Belfast, BT9 5AG Belfast, Northern Ireland, United Kingdom

<sup>b</sup> Technische Universität Hamburg-Harburg, Institut für Fluidodynamik und Schiffstheorie, Am Schwarzenberg, D-21073 Hamburg, Germany

## ARTICLE INFO

### Article history:

Received 5 April 2016

Revised 3 June 2016

Accepted 15 July 2016

Available online 25 July 2016

### Keywords:

Oscillating wave surge converter

Computational fluid dynamics

Wave excitation

Wave energy converter

Control theory

Resonance

Power take-off

## ABSTRACT

Oscillating wave surge converters are a promising technology to harvest ocean wave energy in the near shore region. Although research has been going on for many years, the characteristics of the wave action on the structure and especially the phase relation between the driving force and wave quantities like velocity or surface elevation have not been investigated in detail. The main reason for this is the lack of suitable methods. Experimental investigations using tank tests do not give direct access to overall hydrodynamic loads, only damping torque of a power take off system can be measured directly. Non-linear computational fluid dynamics methods have only recently been applied in the research of this type of devices. This paper presents a new metric named wave torque, which is the total hydrodynamic torque minus the still water pitch stiffness at any given angle of rotation. Changes in characteristics of that metric over a wave cycle and for different power take off settings are investigated using computational fluid dynamics methods. Firstly, it is shown that linearised methods cannot predict optimum damping in typical operating states of OWSCs. We then present phase relationships between main kinetic parameters for different damping levels. Although the flap seems to operate close to resonance, as predicted by linear theory, no obvious condition defining optimum damping is found.

© 2016 The Authors. Published by Elsevier Ltd. This is an open access article under the CC BY license (<http://creativecommons.org/licenses/by/4.0/>).

## 1. Introduction

Among the wide range of wave energy converters (WECs) the class of oscillating wave surge converters (OWSCs) has significantly gained importance in the last years. Both, on scientific and commercial level concepts of OWSCs have been presented and are subject to ongoing research. Some examples to be mentioned are WaveRoller by AW-Energy [1,2], bioWAVE (BioPower Systems) or Oyster by Aquamarine Power [3]. In contrast to e.g. heaving buoys or oscillating water column devices, OWSCs are driven by the horizontal particle motion of the wave. They are therefore usually deployed in the near-shore environment where the horizontal particle motion is amplified [4].

Subject of this investigation is a generic flap-type OWSC similar to Oyster. It consists of a buoyant surface-piercing flap that pitches back and forth around a hinge close to the seabed driven by the torque of incoming waves. Two hydraulic pistons attached to the landward side of the flap serve as a power take-off system (PTO). During operation they act a constant damping torque on the device that is in phase but acts in opposite direction than velocity. The pressurised water powers a

\* Corresponding author.

E-mail address: [p.schmitt@qub.ac.uk](mailto:p.schmitt@qub.ac.uk) (P. Schmitt).

hydro-electric generator on-shore. For further information on the technical details of the device and its development, see [5,6].

One area of interest of OWSC hydrodynamics is the instantaneous characteristics of wave excitation or the torque exerted by the wave on the device while it oscillates freely or damped by the PTO. Specific features of interest are its characteristic course during a wave cycle, its magnitude and its phase relations to other kinetic quantities. It might be unexpected in the first place that such fundamental quantities have not been explicitly identified so far, even though they are crucial for the accuracy of power prediction models or detailed load analysis. However, a closer look at common research techniques reveals that the reason therefore lies in their inherent limitations. Experimental wave tank tests suffer from a lack of appropriate measuring techniques to capture the instantaneous wave torque and the range of validity of linear BEM codes like WAMIT or NEMOH is typically exceeded in operating conditions due to non-linear wave characteristics or high rotation amplitudes of the device.

Many of these limitations can be overcome by the use of fully-viscous non-linear CFD models that model the device and the surrounding fluid. Recent studies prove the feasibility and accuracy of RANS finite volume codes using the volume of fluid method (VOF) to model the free surface interface. While [7] present qualitative comparison with experimental data in monochromatic seas, [8] present simulations in irregular waves similar to typical operating conditions and quantify differences between experimental and numerical data with a model coefficient of 0.98.

Despite the high detail and accuracy of such methods, long-term performance modelling is not feasible for engineering tasks due to the high computational cost [9]. Their application should thus aim at a better overall understanding of the hydrodynamics of OWSCs in order to improve the accuracy of existing simple models or support specific engineering tasks.

In this paper we first present a review of previous investigations on the topic of wave excitation and PTO optimisation and state the limitations that emanate from other applied methods. We then give a brief description of the applied CFD model and outline the computation of wave torque based on the cell-wise data provided by the numerical simulations. Furthermore we discuss the influence of PTO torque on the magnitude and phase relations of wave torque. The latter is based on power optimisation test series of an OWSC operating in two representative monochromatic waves. For the sake of clarity the degrees of freedom and certain descriptive terms of an OWSC are given in Fig. 3.

## 2. Definition of wave torque

Before discussing the wave excitation of an OWSC, we define this term for our purpose in more detail. Within literature several terms such as 'fluid pressure torque', 'hydrodynamic torque' or 'wave excitation torque' are used that often mean the same thing but sometimes differ in crucial details.

In this paper we will use the terms *hydrodynamic torque* and *wave torque*.

The term *hydrodynamic torque*  $T_h$  shall correspond to the overall torque the surrounding water acts on the device. An equation of motion directly equivalent to Newton's famous second law of motion is written as follows:

$$T_h = (I)\ddot{\theta} + T_g + T_{PTO}, \quad (1)$$

with the inertia  $I$  of the flap structure,  $\ddot{\theta}$  the acceleration of the flap,  $T_g$  the torque due to gravitation and  $T_{PTO}$  the torque component due to the power take off system. This formulation is used for example in CFD simulations, where the overall hydrodynamic forces are available.

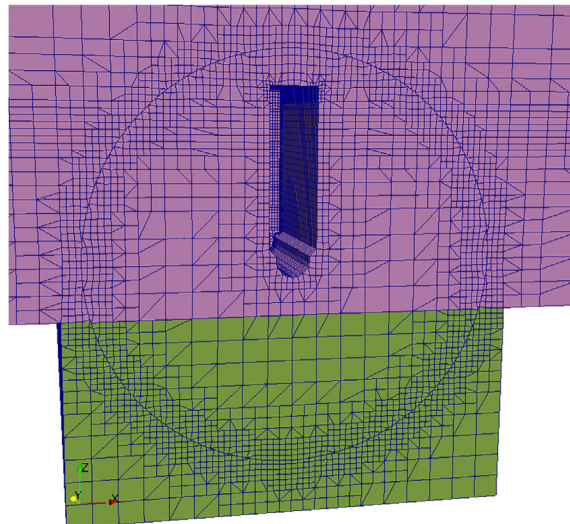


Fig. 1. Mesh around the flap. Colour indicates the variable sand used to model the sea floor inside the rotating domain.

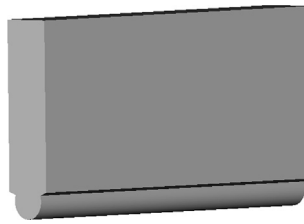


Fig. 2. CAD drawing of the investigated OWSC model.

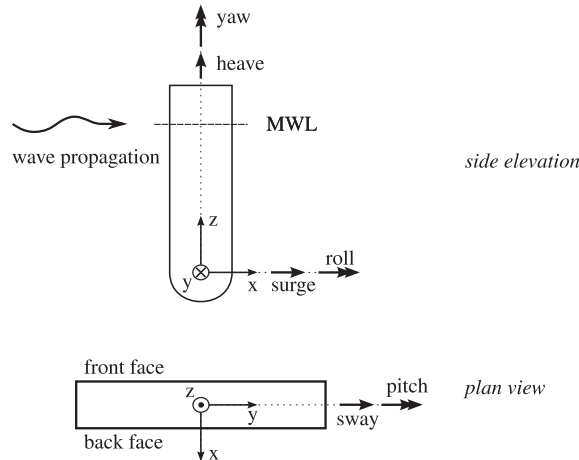


Fig. 3. Conceptual sketch of an OWSC indicating the definition of coordinates and degrees of freedom. The hinge coincides with the  $y$ -axis.

Fig. 4 shows surface elevation  $\eta$  beside the flap, the rotation angle  $\theta$  and rotational velocity  $\dot{\theta}$  and normalised traces of  $T_h, T_g, T_{PTO}$  and the resulting torque  $T_r$  driving the flap motion over one wave period for an almost optimally damped case.

The rotation angle is about a quarter period ahead of the wave crest. The largest amplitude can be observed for the hydrodynamic torque, driving the motion roughly in phase with the surface elevation. Note, that the shape is not similar to the surface elevation but exhibits secondary peaks when the damping torque is changing. The power take off system simulated here assumes a constant value and acts against the flap rotation. For low rotational velocities the damping torque can be seen to drop towards zero. The exact details of the implementation are given later in Section 4.1.  $T_g$  depends (for a fixed position of the centre of gravity relative to the body) only on rotation angle and thus follows the rotation trace. The resulting torque amplitude  $T_r$  is only about 20% of the exciting hydrodynamic torque  $T_h$  and does not resemble the surface elevation in shape.

For historical reasons, especially in linear potential theory as employed in boundary element codes like WAMIT or NEMOH the hydrodynamic forces are often split into individual components. The wave excitation torque  $T_e$  is only the component of the wave acting on a fixed flap and calculated independently of the radiation torque, caused by the flaps' motion in still water. The radiation torque is typically split into components in phase with acceleration (Added Inertia  $I_a$ ), velocity (added damping ( $T_d$ )) and position (hydrostatic stiffness and gravity forces). In a linear framework, these properties depend only on frequency and scale linearly with wave height. Under the linear assumption, an optimum linear damping term can be derived for each wave frequency, as presented for example by [10–12]. It should be noted though, that recent research has shown significant deviations between linear theory and OWSCs in operating conditions. [13,14] presented experimental comparisons with BEM tools for excitation torque, added inertia and damping. Deviations of more than 20% for OWSCs operating with rotation angles of more than 15° were commonly found. A discussion of the validity of the assumption of non-linearity and a derivation of non-linear drag coefficients using numerical and experimental free decay tests can also be found in [15].

Many authors have used the standard linear convention for previous studies of OWSCs, e.g. [16,3,17] who defined the equations of motion as follows:

$$T_e = (I + I_a)\ddot{\theta} + k_p \sin \theta + T_d + T_{PTO}, \quad (2)$$

The term *hydrodynamic torque* corresponds to the overall torque the surrounding water acts on the device. Thus it comprises the incident excitation  $T_e$ , the inertia of the surrounding fluid, the restoring force due to the flap's hydrostatic stiffness  $k_p$  and the damping torque  $T_d$  that again combines damping due to wave radiation and in some cases additional non-linear terms. Speaking in terms of Eq. (2) yields

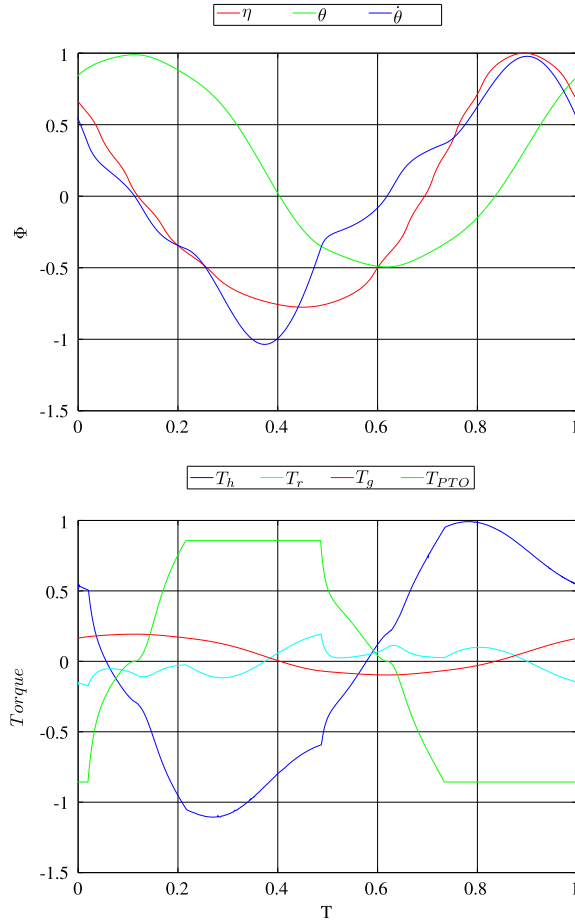


**Fig. 4.** Normalised surface elevation, kinematic quantities of the flap (top) and torque components (bottom) over one wave cycle for optimum damping as obtained from CFD simulations ( $H = 2.1$  m).

$$T_h = T_e - I_a \ddot{\theta} - k_p \sin \theta - T_d. \tag{3}$$

As *wave torque*  $T_w$  we shall define the sum of all kinetic quantities that are only acting due to the presence of the wave and the resulting movement of the device. Since the restoring moment  $T_{kp} = -k_p \sin \theta$  is purely a function of the shape and weight distribution of any flap structure, but independent of the flap’s dynamics, it will be excluded. The *wave torque* is thus given by

$$T_w = T_h - T_{kp} = T_e - I_a \ddot{\theta} - T_d. \tag{4}$$

It becomes obvious that the wave torque does not agree with the excitation torque as given in Eq. (2).  $T_{kp}$  is evaluated for still water surface and a static property. The evaluation is not affected by possible non-linear effects as the traditional  $T_e$  is. We will therefore use  $T_w$  to describe wave excitation in the following.

It should be noted, however, that the description of phase related phenomena such as resonance can deviate between approaches using  $T_e$  or  $T_w$ . This is due to the hydrodynamic damping  $T_d$  that is assumed to be in phase with velocity. With it being included in  $T_w$  the phase of the wave torque with respect to other kinetic quantities will differ from that of  $T_e$ . After all this approach will be based on an equation of motion given by

$$T_w = I \ddot{\theta} - T_{kp} + T_{PTO}. \tag{5}$$

### 3. Wave excitation studies

#### 3.1. Experimental studies

Within numerous investigations wave tank tests proved to be a suitable method for parameter studies [e.g. 6] and provided data to develop a fundamental understanding of the underlying hydrodynamics [18]. The latter includes aspects such as power capture and its dependencies on wave characteristics, loading or the adjustment of PTO torque to name a few.

Most set-ups for the physical modelling of OWSCs can capture the kinematics of the device as well as certain internal forces and moments. Models are therefore equipped with rotation sensors, accelerometers, torque transducers in the bottom tube (along the hinge axis) and 6-DOF load cells measuring the foundation loads. We shall call this the *standard* set-up in the following as most experimental studies are based on such or similar equipment, see for instance [18–21]. A look upon the position of the kinetic sensors within the overall mechanical system (flap, bottom tube and foundation) reveals what can be measured and why the instantaneous wave torque or the hydrodynamic torque can not be measured.

Torque transducers in the bottom tube only measure the torque propagating through this component. Since the PTO is commonly modelled by brake systems attached to the bottom tube the measured torque directly corresponds to the PTO torque. The same applies to 6-DOF load cells. They carry the substructure the bottom tube and flap are mounted on. Thus it can measure the external forces in all degrees of freedom except for pitch where again it only measures the applied PTO torque [22].

The only way to overcome the above-mentioned limitations is the application of pressure sensors on the flap's surface. This, however is technically challenging. Sensors not only need to fulfil the metrological requirements but also have to be waterproof and of sufficiently small longitudinal size. Note that model flap thickness' measure about 0.08 ... 0.15 m depending on the Froude-scaling factor  $\lambda = 25 \dots 40$  in typical wave tank experiments. Furthermore a single pressure sensor only yields data for a single point. Hence satisfactory results in terms of the hydrodynamic torque can only be provided by a large number of sensors that allows for a good interpolation. [23] performed wave tank tests using a fixed flap model with 17 sensor positions. Interpolated hydrodynamic torque time series were compared to the torque measured by torque transducers in the bottom tube showing a coefficient of determination [e.g. 24] of 0.94.

The only studies known to the authors using pressure sensors on fully three dimensional flaps were performed by [25,21,26]. Only the former also computed hydrodynamic torque time series interpolating signals of 13 pressure sensors and assuming symmetry over the front and back face. Since the experiments were based on the standard set-up described above no reference torque was provided. Thus the accuracy of the results can hardly be judged. After all we have to bear in mind that the pressure difference between the front and back face driving the flap is very small relative to the absolute pressures measured on the flap's surfaces. Consequently the effects of error propagation on the resulting computed hydrodynamic torque can be severe.

### 3.2. Numerical studies

For most investigations of OWSC BEM codes like *WAMIT* or *NEMOH* can be an efficient alternative to physical tests. They are well-established for the computation of hydrodynamic coefficients such as added mass and can be applied for parameter studies [e.g. 27].

Henry [18] used *WAMIT* to compute the wave excitation torque (see  $T_e$ , Eq. (2)) for different flap dimensions in order to determine the optimal flap height and width for certain wave climates. Similar computations were performed by [16,20] to be fed into numerical single-DOF oscillator models.

The work by [10] also used linear potential theory to derive the hydrodynamic coefficients, but by using the retardation integral was able to apply non-linear PTO damping in time domain. He investigated active bipolar damping and described in detail the equivalent of an additional pitch stiffness due to ideal damping, leading to increased power output by improving the phase relationship between angular velocity of the flap and wave torque.

Naturally all of the above-mentioned studies are constrained by the limits of applicability of potential flow and linear wave theory. With respect to OWSCs a major drawback thereof is the applicability to small rotation angles only. Even during normal operation this assumption is often violated, typical angles of rotation in production seas exceed 30°. Furthermore [23] showed that the underlying linear assumptions also do not hold for long wave periods, especially for large Stokes parameters.

Computational fluid dynamics tools like OpenFOAM can replicate experiments tank testing up to the level of the experimental accuracy. At the same time, they can provide access to all field variables in all locations, making them the tool of choice for the current investigation.

## 4. Methods

### 4.1. CFD Set-up

Simulations were performed using the method described in detail in [8], with the addition of a model for the PTO system. A PTO torque can be specified as fixed value  $M_{Dconst}$ , or as varying linearly  $\alpha$  or quadratically  $\beta$  with the rotation velocity  $\dot{\theta}$ . The PTO torque  $T_{PTO}$  acting on the flap is then computed according to the following equations:

$$T_{PTO} = -\dot{\theta}(\alpha + |\dot{\theta}|\beta) \quad (6)$$

$$\text{if } (M_{Dconst} > \epsilon_{Num}) \quad (7)$$

$$T_{PTO} = -\text{sign}(\dot{\theta})\min(|T_{PTO}|, |M_{Dconst}|) \quad (8)$$

with  $\epsilon_{Num}$  being a very small number. When a constant damping torque is defined, the quadratic (or linear) coefficient  $\beta$  (or  $\alpha$ ) should be chosen so that the constant damping is smaller over most of the rotation, otherwise the setting has no effect. This implementation allows to simulate different settings for the increase in damping torque over rotational velocity. In this work constant damping torque was modelled. The settings used are provided in the appendix in Tables A.1 and A.2.

A minor difference to the method described in [8] is the use of symmetry conditions along the centre of the numerical tank. Typical mesh sizes are about 200,000 cells. Fig. 1 shows the mesh around the flap, with refinement areas around the moving structure, the cylindrical, rotating domain and the water surface. A variable time-step with the Courant number limited to a maximum value of 0.3 was used. Simulations were run for 15 s simulation time (more than 10 wave cycles at 40th scale) to reach steady oscillations of the OWSC. On 24 cores a single simulation took about 24 h.

#### 4.2. The computation of wave torque

Within the solver of the *OpenFOAM* set-up the equation of motion of the flap with its surface being discretized by  $n$  cells is represented by

$$I \cdot \ddot{\theta} = mg \|\vec{CoG}\| \sin(\theta) + \sum_{i=1}^n (M_{p,i} + M_{\tau,i}) + T_{PTO}, \tag{9}$$

where  $m$  is the mass of the flap and  $\vec{CoG}$  is the distance from the centre of gravity of the flap to the pivot.  $M_{p,i}$  and  $M_{\tau,i}$  are the moments due to pressure and viscous shear stress, respectively, related to a cell  $i$ .

Consulting Eqs. (2) and (3) it becomes obvious that

$$T_h = \sum_{i=1}^n (M_{p,i} + M_{\tau,i}). \tag{10}$$

In order to obtain the wave torque  $T_w$  with respect to Eq. (4) the restoring moment  $T_{kp}(\theta)$  has to be subtracted.

The latter is computed independently from the actual CFD simulation by a supplementary *python* script. Results for the flap investigated are given in Fig. C.12. The geometry is directly imported from an STL (stereo lithography) file that is also used for the mesh generation.

Since only the hydrodynamic torque  $T_h$  is computed by the solver during run time,  $T_w(t)$  is calculated in the post processing using  $T_{kp}(\theta)$  and the rotation angle  $\theta(t)$

$$T_w(t) = T_h(t) - T_{kp}(\theta(t)). \tag{11}$$

#### 4.3. Model and case description

As this investigation focuses on the general characteristics of the wave excitation of an OWSC a simple generic box-shape was chosen, see Fig. 2.

The outer dimensions as well as its water depth and hinge position but not its weight are those of Oyster 800 by Aquamarine Power Ltd. and are given in Fig. 5.

Two cases of monochromatic waves of height  $H = 2.1$  m and  $H = 3$  m are simulated. The wave period is  $T = 9$  s for both cases. With respect to occurrence and performance these represent typical wave climates where OWSCs produce the majority of their annual power [6,5].

It should also be noted, that the OWSC does not operate in resonance, like other wave energy converters. The natural period is the frequency with which the (undamped) body will oscillate if excited and let free to move in still water. A heaving buoy, for example will produce most power, when its' natural frequency is close to the exciting wave frequency (resonance). The natural frequency of a submerged body depends on the water accelerated due to the bodies' motion (added mass/inertia). The natural pitching period of the flap  $T_n$  according to [17], given by

$$T_n = 2\pi \sqrt{\frac{I + I_a(T)}{k_p}} \tag{12}$$

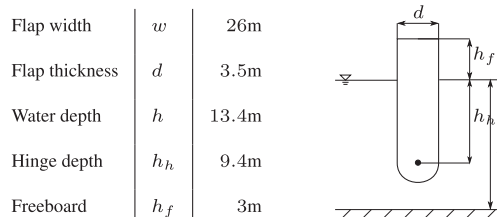


Fig. 5. Outer dimensions and positioning of the model.

is 10.4 s. In earlier work mostly flaps with significantly larger pitch stiffness and Eigenperiods of around 20 s were investigated. The flap here is based on the setup used by [15], who obtained an Eigenfrequency of about 14s in experimental and numerical free decay tests. The added inertia  $I_a(T)$  was computed with *NEMOH* and the pitch stiffness derived  $k_p$  from the above-mentioned computation of  $T_{kp}$ , with

$$k_p = \frac{\partial T_{kp}^0}{\partial \theta}. \quad (13)$$

$I_a$  was obtained using the boundary element code *NEMOH*, while the pitch stiffness was evaluated using custom tools written for freeCAD. Data is given in more detail in the appendix, see Figs. B.11 and C.12. The Eigenfrequency is thus almost 15% above the wave frequency used in these tests. Within a certain wave climate the performance of an OWSC strongly depends on the applied PTO torque. [18] showed that the power curve ( $RMS(P)$  vs.  $T_{PTO}$ ) of an OWSC, with

$$P = |\dot{\theta} \cdot T_{PTO}|, \quad (14)$$

can be approximated by a parabola which allows for quadratic interpolation in order to find the optimal PTO torque within a wave climate. The effects of different PTO torques on the wave torque will therefore be discussed with respect to a power curve based on several applied PTO torques covering over, under and optimally damped states.

## 5. Results and discussion

Unless otherwise stated, all results presented here are shown for the 2.1 m wave height. Results of the respective simulations for 3 m waves are presented in the appendix. Being most important for the power output, the velocity and the wave torque at all damping torques are given in Fig. 8. As a reference point the surface elevation in the far field is given additionally. Fig. 7 shows all simulated damping levels over the corresponding power output. The curve is an inverted parabola fitted to the data points. The different PTO damping levels will be referred to as D0 to D5 with increasing damping levels, beginning with the undamped case D0. It shows that the optimal damping measures  $T_{PTO} \approx 8.5MN\ m$ . D3 and D4 are consequently close to the optimum whereas D1 and D2 are clearly underdamped and D5 and D6 are overdamped.

### 5.1. Comparison with linear model

Earlier studies employing linearised tools in frequency domain obtained ideal linear damping coefficients. The technical realisation of such damping methods is difficult, due to the large amplitudes. Technical realisations of OWSC PTOs have to date all been based on hydraulic systems, best simulated by a fixed torque as discussed above. The linear damping coefficient scales with wave amplitude and since it is a sinusoidal signal cannot be compared directly to the constant amplitude damping used in real implementations or the simulations presented here. While it would be possible to run linear damping in CFD it is beyond the scope of this paper. However, it should be noted that the optimum PTO damping, according to linear theory, scales with wave height. The ratio between the wave heights of  $\frac{3}{2.1} = 1.4286$  differs almost 13% from the ratio of the two ideal damping levels (1.2625) found in the non-linear simulations, thus highlighting the limitations of linear tools for the simulation of OWSCs in operating conditions.

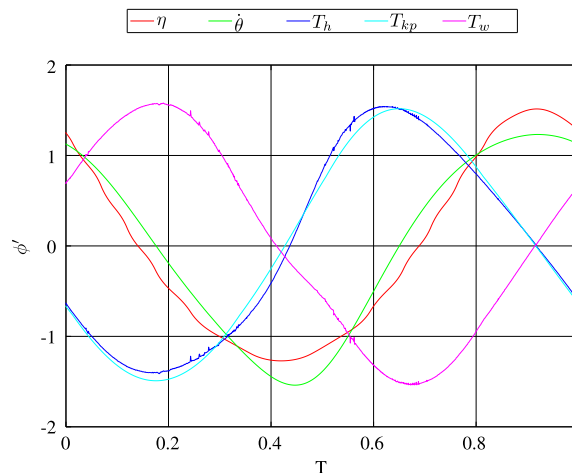


Fig. 6. Normalised kinetic properties  $\phi' = \phi/\bar{\phi}$  with  $\bar{\phi} = RMS(\phi)$  during one wave cycle ( $H = 2.1$  m).

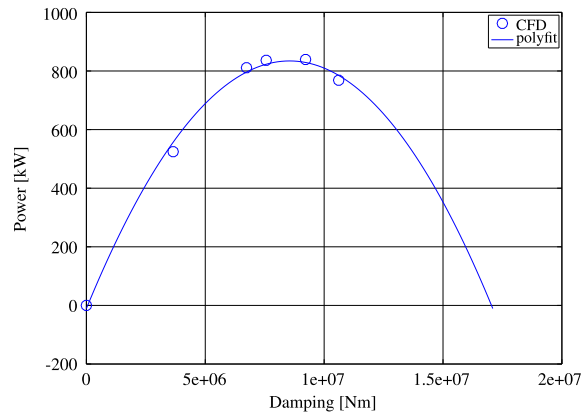


Fig. 7. Power curve with PTO dampings D0 to D6 ( $H = 2.1$  m).

## 5.2. Phase relationships

To outline the starting point of the discussion normalized time traces of the major kinetic parameters  $\phi$  of the undamped ( $T_{PTO} = 0$ ) OWSC as well as the surface elevation  $\eta$  on the hinge axis in the far field are given in Fig. 6.

The velocity of the flap lags wave torque by  $0.26T$  corresponding to a phase angle of  $94^\circ$ . Hence the flap is not resonant which agrees with the computed natural period presented in Section 4.3.

In the following we will discuss the effects of different applied PTO torques.

It becomes obvious that the application of damping torque first of all changes the characteristic of the acting wave torque. Starting from the sinusoidal shape of the undamped case it becomes more square-shaped the higher the applied damping torque. At the same time it increases in magnitude. Both is based on the fact that the flap imposes a higher resistance on the wave characterised by the constant PTO torque. Furthermore its phase angle with respect to the unaffected surface elevation decreases.

The magnitude of velocity decreases with increasing damping torque. This appears to be straightforward since the increasing resistance of the flap on the incoming wave is based on the fact that its rotation is constrained by the PTO damping. Moreover the phase lag of the velocity with respect to surface elevation is decreased as with the wave torque.

In order to evaluate the phase relations the lags between velocity, rotation, surface elevation and wave torque were computed applying cross correlation [28] and converted to phase angles with respect to the wave period, see Fig. 9. The ideal damping is shown by a vertical black line.

We can see that the phase angles between velocity and surface elevation  $\varphi_{\dot{\theta},\eta}$  and rotation and surface elevation  $\varphi_{\theta,\eta}$  increase with increasing PTO torque. Most importantly for the performance of the flap the phase angle between velocity and wave torque  $\varphi_{\dot{\theta},T}$  decreases in magnitude. The resulting phase lead of velocity towards wave torque at D6 is almost  $0^\circ$  starting from an initial undamped phase lead of  $110^\circ$ . Thus the flap approaches a resonant state with increasing PTO torque.

This investigation shows that the application of PTO damping torque results in a crucial manipulation of incoming waves. The flap's increasing diffraction of incident waves both increases wave torque and shifts its phase with respect to the flap's velocity. The state of the flap with optimal PTO damping torque in the investigated case is indeed relatively close to resonance as the phase of the wave torque is almost in phase with the flap's angular velocity ( $\varphi_{\dot{\theta},T}^{P_{max}} \approx 15^\circ$ ). Talking in terms of power output the optimally damped flap rotates with a small velocity (compared to the undamped case) that is almost in phase with a significantly increased exciting wave torque driving a PTO with high level of damping. That near resonance is good for power output might have been expected, but these results highlight another problem. Ideal damping is indicated by near resonance but at higher damping levels, the phase angle further decreases but so does power output. The same can be observed for the higher wave height in Fig. 10 and indicates that phase relations are not sufficient to find optimum damping settings.

It might be assumed that the residual phase difference in the optimally damped state is related to the discrepancy between the undamped natural period of the flap ( $T_n = 10.4$  s) and the period of the tested wave ( $T = 9$  s). This has to be clarified by future investigations.

Interestingly, the phase between wave torque and surface elevation of the undisturbed wave crosses 0, changing from negative to positive, close to the ideal damping level for both wave heights investigated. The reason for this is unclear and further simulations are required to investigate if this holds true for other wave frequencies.

Clabby et al. [29] provides a similar investigation using experimental tank tests of a 20th scale model of Oyster 1 in a monochromatic wave of  $H = 3.30$  m and  $T_m = 10.78$  s. Even though a comparison is not straightforward the results suggest the same conclusion. Due to the experimental set-up wave torque could not be measured for reasons described earlier. Consequently the phase angle of surface elevation and rotation is presented. It is shown that the phase angle of surface elevation and rotation reduces when increasing damping torque towards optimum. This generally coincides with the results found for

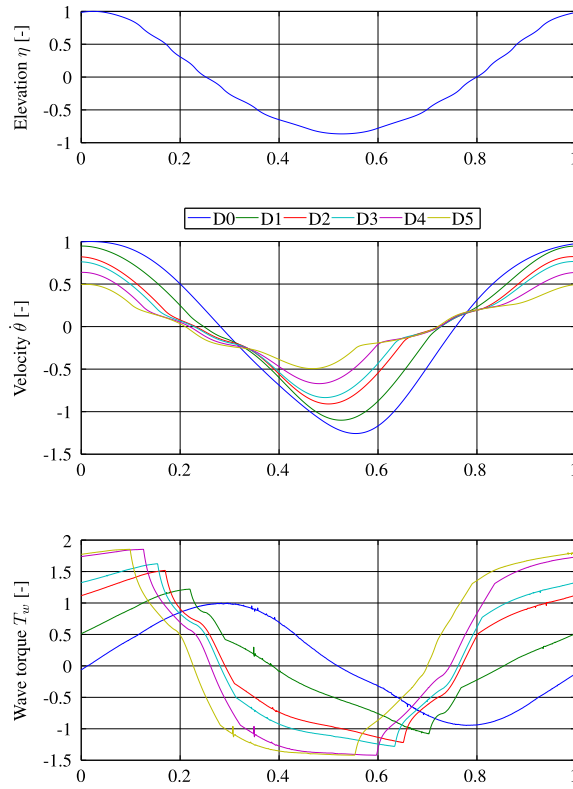


**Fig. 8.** Surface elevation  $\eta$  in the far field (top). Rotational velocity  $\dot{\theta}$  (middle) and wave torque  $T_w$  (bottom) during one wave cycle with different applied PTO torques ( $H = 2.1$  m).

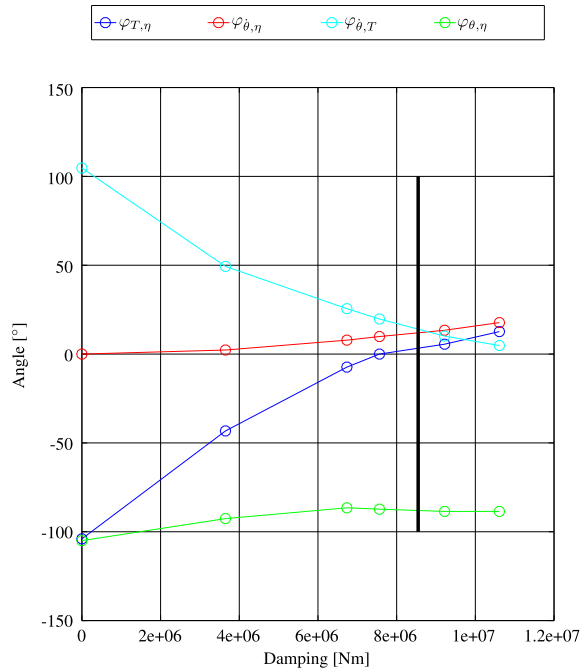


**Fig. 9.** Phase angles of kinetic properties over applied external damping  $T_{pto}$ , with  $\varphi_{\phi_1,\phi_2} = \varphi_{\phi_1} - \varphi_{\phi_2}$ . The vertical black line indicates optimum damping ( $H = 2.1$  m).

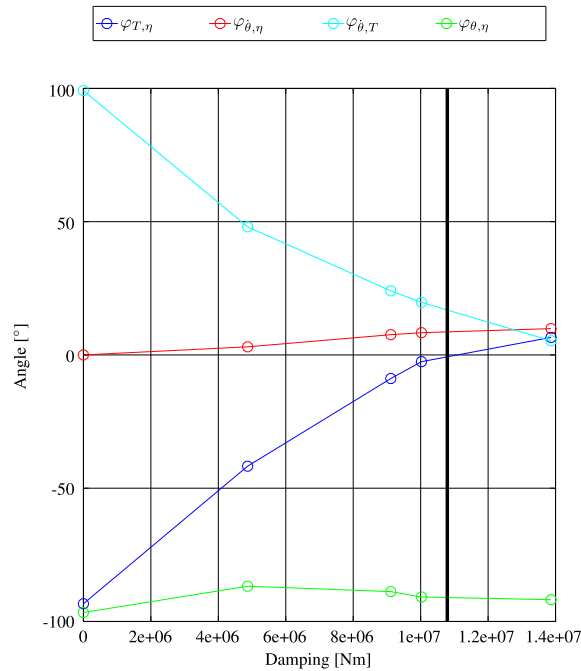


**Fig. 10.** Phase angles of kinetic properties over applied external damping  $T_{PTO}$ , with  $\varphi_{\phi_1,\phi_2} = \varphi_{\phi_1} - \varphi_{\phi_2}$ . The vertical black line indicates optimum damping ( $H = 3$  m).

surface elevation and rotation in this investigation. We might thus assume that the phase shift of wave torque and velocity is similar to the one found in this work. Unfortunately the investigated flap is smaller in width and the wave differs in height and period. Thus any more explicit comparison using parameters given in both investigations can not be made.

**6. Conclusion**

In this paper we have presented a novel method to determine the instantaneous wave excitation of an OWSC. RANS CFD simulations were used for the first time to find the optimum damping settings for an OWSC in a certain wave condition. These simulations show the same effects of different damping levels on power production than experimental tests and can be used to find optimum damping levels. Non-linear simulations show that even in normal operating conditions ideal damping settings do not scale linearly with wave height as linear theory predicts. While the OWSC’s eigenfrequency differs from the incoming waves, so perfect resonance cannot be achieved, simulations show a significant change in the characteristic course of the wave torque with increasing PTO torque. As predicted by linear theory a decrease in the phase shift between the OWSC’s velocity and the wave excitation torque can be observed with increasing damping levels. When optimally damped though, the phase angle has not yet reached zero. Power output decreases with further damping and even closer resemblance to a resonant state. Phase relationships alone do not seem to be sufficient to identify optimum damping states.

**Acknowledgement**

Henrik Asmuth was funded by Aquamarine Power Ltd. and the project was enabled through EPSRC grant EP/M014738/1. Their support is much appreciated.

**Appendix A. Damping settings used for 40th simulations**

**Table A.1**  
Damping coefficients used for different PTO settings ( $H = 2.1$  m).

Case	$\beta$	$M_{Dconst}$
D0	0	0
D1	25	1.5
D2	25	3
D3	25	3.5
D4	25	4.5
D5	25	5.5

**Table A.2**  
Damping coefficients used for different PTO settings ( $H = 3$  m).

Case	$\beta$	$M_{Dconst}$
D0	0	0
D1	25	2
D2	25	4
D3	25	4.5
D4	25	7

**Appendix B. Data obtained with NEMOH BEM**

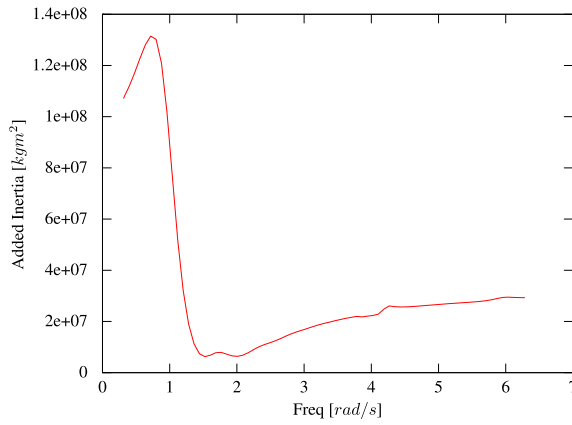


**Fig. B.11.** Added inertia over frequency as obtained from NEMOH.

**Appendix C. Hydrostatic pitch stiffness**

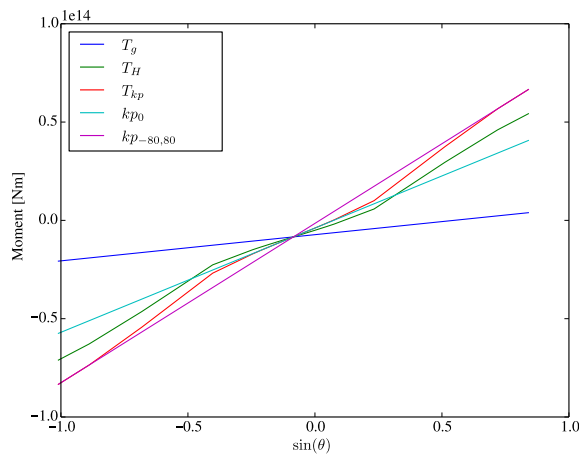


**Fig. C.12.** Hydrostatic pitching moment and its components over the sinus of the flap angle. Additionally the linear approximation for small  $kp_0$  and large  $kp_{-80,80}$  rotation amplitudes is given.

**Appendix D. Additional plots for 3 m wave height**

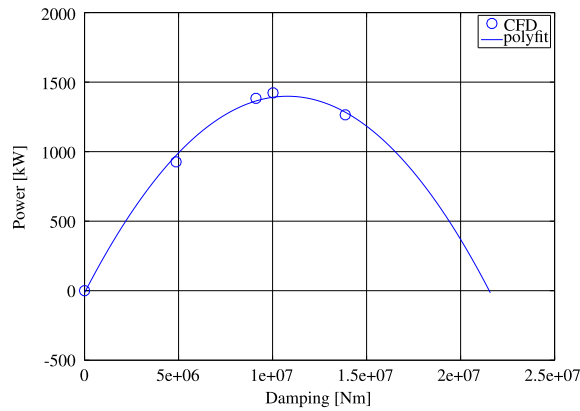


**Fig. D.13.** Power curve with PTO dampings D0 to D5  $H = 3$  m.

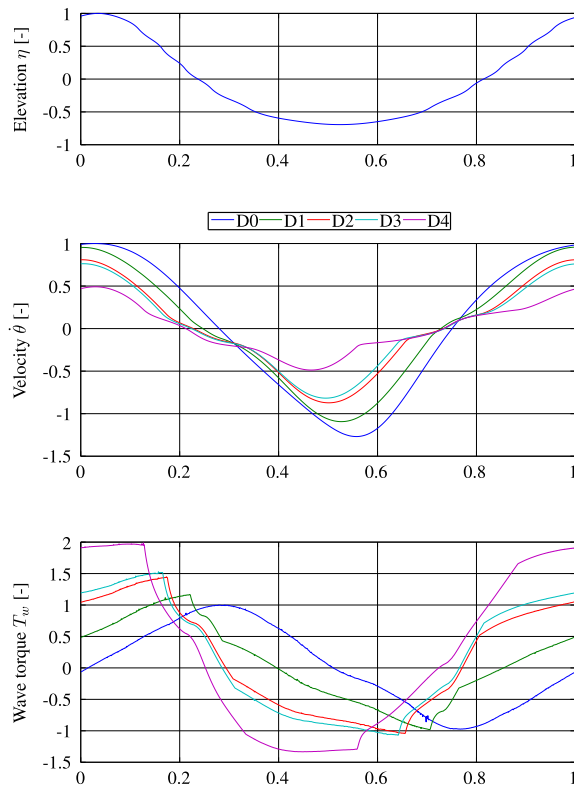


**Fig. D.14.** Surface elevation  $\eta$  in the far field (top). Rotational velocity  $\dot{\theta}$  (middle) and wave torque  $T_w$  (bottom) during one wave cycle with different applied PTO torques  $H = 3$  m.

**References**

- [1] T. Mäki, T. Mucha, M. Vuorinen, Waveroller one of the leading technologies for wave energy conversion, ICQE 2014.
- [2] J. Lucas, M. Livingstone, M. Vuorinen, J. Cruz, Development of a wave energy converter (WEC) design tool—application to the waveroller wec including validation of numerical estimates, ICQE 2012.
- [3] T. Whittaker, David Collier, Matt Foley, M. Osterried, A. Henry, M. Crowley, The development of oyster – a shallow water surging wave energy converter, in: 7th Annual European Wave & Tidal Energy Conference, 2007.

- [4] M. Folley, T. Whittaker, A. Henry, The effect of water depth on the performance of a small surging wave energy converter, *Ocean Eng.* 34 (2007) 1265–1274.
- [5] T. Whittaker, M. Folley, Nearshore oscillating wave surge converters and the development of oyster, *Philos. Trans. R. Soc. A* 370 (2012) 345–364.
- [6] L. Cameron, R. Doherty, A. Henry, K. Doherty, J. van't Hoff, D. Kaye, D. Naylor, S. Bourdier, T. Whittaker, Design of the next generation of the oyster wave energy converter, in: *Proceedings of the 3rd International Conference on Ocean Energy*, 6 October, Bilbao.
- [7] Y. Wei, A. Rafiee, A. Henry, F. Dias, Wave interaction with an oscillating wave surge converter, part i: viscous effects, *Ocean Eng.* 104 (2015) 185–203, <http://dx.doi.org/10.1016/j.oceaneng.2015.05.002>. cited By 0, URL <http://www.scopus.com/inward/record.url?eid=2-s2.0-84936880408&partnerID=40&md5=e2c579932d459660fbfc591ce5a7b14>.
- [8] P. Schmitt, B. Elsässer, On the use of OpenFOAM to model oscillating wave surge converters, *Ocean Eng.* 108 (2015) 98–104, <http://dx.doi.org/10.1016/j.oceaneng.2015.07.055>. URL <http://www.sciencedirect.com/science/article/pii/S0029801815003686>.
- [9] P. Schmitt, T. Whittaker, D. Clabby, K. Doherty, The opportunities and limitations of using cfd in the development of waver energy converters, in: *Marine & Offshore Renewable Energy Conference*, London.
- [10] M. Folley, T. Whittaker, The control of wave energy converters using active bipolar damping, *Proc. Inst. Mech. Eng., Part M: J. Eng. Marit. Environ.* 223 (4) (2009) 479–487, <http://dx.doi.org/10.1243/14750902JEME169>. arXiv:<http://pim.sagepub.com/content/223/4/479.full.pdf+html>, URL <http://pim.sagepub.com/content/223/4/479.abstract>.
- [11] J. Falnes, *Ocean Waves and Oscillating Systems*, Cambridge University Press, 2002.
- [12] E. Renzi, A. Dias, Hydrodynamics of the oscillating wave surge converter in the open ocean, *Eur. J. Mech. B/Fluids* 41 (2012) 1–10.
- [13] D. Crooks, J. van't Hoff, M. Folley, B. Elsässer, Oscillating wave surge converter forced oscillation tests, in: *Proceedings of the ASME 2016 35th International Conference on Ocean, Offshore and Arctic Engineering*, 2016. under review.
- [14] D. Crooks, T.J. Whittaker, J. van't Hoff, C. Cummins, Experimental validation of numerically generated wave excitation torque on an owsc, in: G. Soares (Ed.), *Renewable Energies Offshore*, Taylor & Francis, Group, London, 2014.
- [15] H. Asmuth, P. Schmitt, B. Henry, A. Elsaesser, Determination of non-linear damping coefficients of bottom-hinged oscillating wave surge converters using numerical free decay tests, in: G. Soares (Ed.), *Renewable Energies Offshore*, Taylor & Francis, Group, London, 2014.
- [16] J. van't Hoff, Hydrodynamic modelling of the oscillating wave surge converter (Ph.D. thesis), Queen's University Belfast, 2009.
- [17] E. Renzi, K. Doherty, A. Henry, F. Dias, How does oyster work? The simple interpretation of Oyster mathematics, *Eur. J. Mech. B. Fluids* 47 (2014) 124–131.
- [18] A. Henry, The hydrodynamics of small seabed mounted bottom hinged wave energy converters in shallow water (Ph.D. thesis), Queen's University Belfast, 2009.
- [19] K. Doherty, M. Folley, D. Doherty, T. Whittaker, Extreme value analysis of wave energy converters, in: *The Proceedings of the 21st (2011) International Offshore and Polar Engineering Conference*, Maui, Hawaii, USA.
- [20] D. Clabby, *Wave energy conversion at prototype and model scales* Ph.D. thesis, Queen's University Belfast, 2013.
- [21] A. Henry, O. Kimmoun, J. Nicholson, G. Dupont, Y. Wei, F. Dias, A two dimensional experimental investigation of slamming of an oscillating wave surge converter, in: *The Proceedings of the 24th (2014) International Offshore and Polar Engineering Conference*, Busan, Korea.
- [22] D. Howard, T. Whittaker, K. Doherty, Foundation load analysis of oyster using a five degree of freedom load transducer, in: *Proceedings of the 8th EWTEC 2009*, Uppsala, Sweden.
- [23] P. Schmitt, S. Bourdier, D. Sarkar, E. Renzi, F. Dias, K. Doherty, T. Whittaker, J. van't Hoff, Hydrodynamic loading on a bottom hinged oscillating wave surge converter, *Proceedings of the Twenty-second (2012) International Offshore and Polar Engineering Conference (2012)* 550–560.
- [24] I. Pardoe, *Applied Regression Modeling: A Business Approach*, John Wiley & Sons, 2012.
- [25] S. Bourdier, K. Abdulla, A. Henry, T. Whittaker, Derivation of wave loads for the design of oscillating wave surge converters, in: *Proceedings of the 10th European Wave and Tidal Energy Conference*, Aalborg, Denmark.
- [26] A. Henry, A. Rafiee, P. Schmitt, F. Dias, T. Whittaker, The characteristics of wave impacts on an oscillating wave surge converter, *Journal of Ocean and Wind Energy* 1 (2) (2014) 101–110.
- [27] M. Folley, T. Whittaker, H. Henry, The performance of a wave energy converter in shallow water, in: *Proceedings of the Sixth EWTEC 2005*, Glasgow, UK.
- [28] J. Buck, M. Daniel, A. Singer, *Computer Explorations in Signals and Systems Using MATLAB*, second ed., Prentice Hall, Upper Saddle River, NJ, 2002.
- [29] D. Clabby, A. Henry, M. Folley, T. Whittaker, The effect of the spectral distribution of wave energy on the performance of a bottom hinged flap type wave energy converter, in: *Proceedings of the ASME 2012 31st International Conference on Ocean, Offshore and Arctic Engineering*.